fortune Journals

Case Report

JOURNAL OF RADIOLOGY AND CLINICAL IMAGING

ISSN: 2644-2809

Topological Approach of 1D Solid Solutions for Singularity in Semicircular Canals

Yves Gourinat[1,*], Arnaud Rolland[1], Thomas Hanchin[1], Marie-Stéphane Guillaumont[1], Quentin Legois[2,3]

Abstract

The dynamic beam equations provide an analytical model and a generic solution for continuous systems. The constants for amplitudes and frequencies are given by the boundary conditions, which are here considered looped, in order to represent a closed element, by topological closure. This type of model is applied to the representation of a semicircular canal. This approach addresses the deformability of this anatomical element, both in Lagrangian solid parts (bone, membranes, intermediate materials) and in fluids (Eulerian pressure waves). The model is proposed for both physiological representation and pathology modeling. The latter is represented by a passive or retroactive singularity. An original analytical approach is thus developed for each segment, representing physiological modes – nodes and bellies - and possible disturbances. The damping entropy is also the subject of a special segmented treatment, to take account of fluid-solid interactions, providing a coherent model. The result is a simplified but robust model that both reproduces the vibro-acoustic modes of the semicircular canal and anticipates the effects of a singular pathology, such as a third window or neuritis. Mathematically, this model opens the way to structural analytical models of the inner ear, and to possible dynamic couplings between equilibration and acoustics.

Keywords: Semi-Circular Canal; Analytical Model; Beam Dynamics; Ring dynamics; Acoustic Model; Longitudinal Dynamics.

Introduction and Context

General introduction

Bar and beam dynamics represents an interesting transition from the discrete harmonic model to the continuous acoustic and structural model. As such, the constitutive equations and their generic solutions - conditioned by boundary conditions are a classic source of analytical development, which we propose to open up in two directions: the topological looping on the one hand, and the introduction of a point singularity on the other. Mathematically, this allows the closing of the system, and the introduction of a punctual perturbation in a continuous dynamic model.

As it turns, this analytical approach using elementary dynamic segments overlaps with a well-known biodynamic system that has been the subject of numerous numerical models, namely the semicircular canals that play a fundamental role in the inner ear, notably for measuring rotation rates. These are complex systems combining fluids (endolymph and perilymph), solids (bone and cartilage) and certain intermediate materials (cup).

Affiliation:

[1]Université de Toulouse – UMR CNRS 5312, ISAE-SUPAERO, TOULOUSE (France).

[2]Service ORL, Otoneurologie et ORL pédiatrique CHU Toulouse Purpan TOULOUSE (France)

[3]Centre de Recherche Cerveau et Cognition, UMR5549, CNRS, TOULOUSE (France)

Corresponding author:
Yves Gourinat, Université de Toulouse, ISAE-SUPAERO, Toulouse, France.

Citation: Yves Gourinat, Arnaud Rolland, Thomas Hanchin, Marie-Stéphane Guillaumont Quentin Legois. Topological Approach of 1D Solid Solutions for Singularity in Semicircular Canals. Journal of Radiology and Clinical Imaging. 7 (2024): 99-111

Received: November 02, 2024
Accepted: November 11, 2024
Published: November 27, 2024

Gourinat Y, et al., J Radiol Clin Imaging 2024
DOI:10.26502/jrci.2809102

Numerous numerical models of the semicircular canals have been proposed, providing a fairly convincing representation of endolymphic and perilymphic physiology. However, the disturbances induced by the main pathologies linked to the semicircular canals remain tricky to observe and model, which justifies the implementation of an analytical model, which is the subject of this article. Fundamentally, this type of model is relatively accurate, but its conceptual robustness offers the advantage of being able to introduce at will perturbations representing the influence of various pathological derangements. The proposed approach is therefore valid for modeling the sensitivity of pathologies on dynamic behavior.

The basic analytical models of semicircular canals generally consider rational, undeformable systems, based on the model of the rotating solid. We thus find the elementary inertial model constructed in rotation around a fixed inertial axis (Huyghens), then the motion of the fixed-point solid (Poinsot, Euler, Lagrange) and finally the gyroscopic extrapolation coupling the effects of precession and nutation (Poisson). In this article, on the other hand, the deformability of the system is taken into account. To remain in the analytical domain, theories of slender solid and fluid bodies are used. More specifically, the equations of bars and beams are exploited, giving the initial preference to the normal force approach, which we will qualify - in the context of beam theory - as a 1D approach.

In this longitudinal 1D approach - in the sense of bars and tubes - it should be noted that the elastic Hooke-Bresse equation solid - and the Helmholtz equation - fluid - lead to a homogeneous d'Alembert equation based on propagation velocity fluid and solid. The generic modal solutions are therefore harmonic and provide an algebraic framework for proposing various set-ups, representing both solid dynamics (longitudinal Lagrangian displacement) and fluid fluctuations (Eulerian pressure variations).

In the first stage, a simple topological loop is created; this closed bar - or ring in longitudinal mode - is the first element that enables us to recover the closed - physiological - vibroacoustic modes, and to experiment with a passive or active singularity. A passive singularity is a simple discontinuity in terms of displacement (in a Lagrangian representation) or pressure (in an Eulerian model). The active singularity consists in inverting the solution at a point (Möbius looping), introducing local retroactivity. It's interesting to note that these two types of singularity have analogies with two types of pathology, windows and neuritis respectively.

The elementary model - which in fact constitutes a first qualitative approach - is then segmented, evoking the various anatomical parts in a fairly realistic way. A number of simplifications are proposed, concerning on the one hand the homogenization of moduli and on the other hand the introduction of a viscosity per segment on the wide parts of the 66 canal.

Observation of the deterministic or chaotic nature of the generic solution then provides information on the consequences of the pathology, and the link with the singular boundary conditions gives clues to possible corrections. It should be noted that this topologically looped longitudinal 1D model provides a first approach to singular pathology and opens the way to more advanced structural 1.5 models.

Medical context

Under normal physiological conditions, sound is a mechanical wave that causes the tympano-ossicular complex to vibrate. Through the articulation between the stapes footplate and the oval window, sound is transmitted from the middle ear to the cochlea (1). The round window, on the other hand, is widely considered to be the anatomical structure that allows for pressure relief by releasing the mechanical energy provided by the ossicular chain to the labyrinthine fluid of the inner ear (2). Hearing encompasses the mechanisms that allow us to perceive the sound waves around us and is made possible by the conversion of these mechanical waves into nerve signals by the basilar membrane, which are then transmitted to the brain (3). Any pathologies or abnormalities in these structures (external, middle, and inner ears) and in the central auditory neural pathways can lead to hearing impairment.

Minor was the first to describe, in 1998, a case series of sound- and/or pressure-induced vertigo in patients with superior semicircular canal dehiscence. The dehiscence's were identified through computed tomographic scans, which revealed the absence of bone overlying the superior semicircular canal on the surface of the temporal bone (4). In addition to sound/pressure-induced vertigo, patients may experience air-conduction hearing loss observed at low frequencies with dehiscences larger than 3 mm. The significance of this air-bone gap is correlated with the size of the dehiscence (5).

The most likely hypothesis is that the dehiscence acts as a "third window" in the inner ear, shunting acoustic energy away from the cochlea at low frequencies, thereby causing hearing loss (6). Some studies have attempted to understand the underlying biomechanical mechanism generating this shunt and have also tried to quantify it. One study specifically investigated the sound-induced displacement velocities of the stapes, umbo, and round window in a temporal bone bank using laser-Doppler vibrometry (6). These measurements were performed on healthy bones considered normal, on the same bones after creating a dehiscence

Gourinat Y, et al., J Radiol Clin Imaging 2024
DOI:10.26502/jrci.2809102

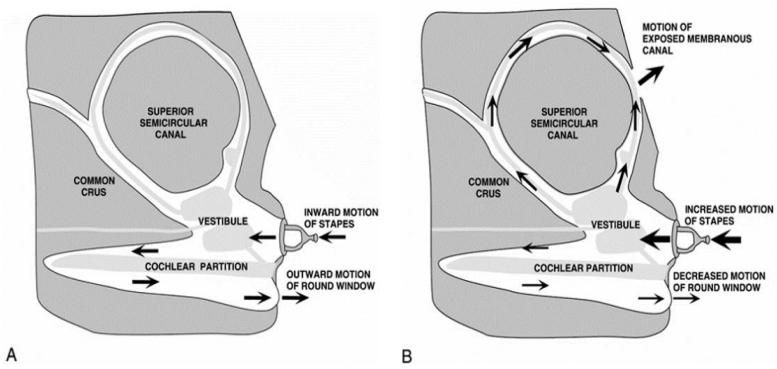

Figure 1: Modeling semi-circular canals for a normal ear (figure extracted from the reference 18)

in the superior semicircular canal, and also with the dehiscence patched. They found that the presence of a dehiscence in the superior semicircular canal led to a significant reduction in sound-induced round window velocity at low frequencies

This allows us to better understand why there can be a air-bone gap result at low frequencies in the presence of a dehiscence, and also why patients might experience vertigo with loud sounds due to the shunting of acoustic energy toward the posterior labyrinth.

Sound energy enters the inner ear via the oval window, causing fluid movement at the location of the bony defect. This generates propagating waves that subsequently lead to mechano-electrical transduction in the vestibular sensory organs through vibration and nonlinear fluid pumping (1). This same team also recorded changes in neural activity in the vestibular pathways in an animal model, evoked by auditory-frequency stimulation (1).

Despite these findings, to our knowledge, no study currently exists to explain the purely biomechanical mechanism of the fluids, and this is what we aimed to address here.

Beam closed ring model

Standard beam solutions

The aim of this section is to study the different resonance modes of a topologically closed beam. To this end, the equations of the dynamics of a rectilinear beam are retained and boundary closure conditions are applied. The beam's radius of curvature is then neglected, which seems to be valid for a beam thickness that is negligible compared with the radius of curvature.

The equation verified by the longitudinal displacement in a rectilinear beam whose lateral shrinkage is neglected is given by:

$$\rho(x)\frac{\partial^2 U_X}{\partial t^2} - E(x)\frac{\partial^2 U_X}{\partial x^2} = 0,$$

where ρ and E are respectively the density and the Young's modulus of the material. This can be rewritten as:

$$\ddot{U}_X - c^2 U_X'' = 0,$$

$$\text{with : } \quad c \equiv \sqrt{\frac{E}{\rho}}, \text{ wave propagation speed in a traction-compression rod;} \qquad \dot{} \equiv \frac{\partial}{\partial t} \text{ and } ' \equiv \frac{\partial}{\partial x}. \tag{1}$$

Closed ring solution

The form of the general solution to the wave equation is valid whether the cross section is constant or not (the material just has to be homogeneous; the solution can be obtained modally by separating the variables:

$$U_X(x,t) = f(x)g(t) \implies c^2\frac{f''}{f} = \frac{\ddot{g}}{g} = -\omega^2 = \text{negative constant.} \tag{2}$$

This general solution is of the form:

$$f(x) = A\cos\Omega x + B\sin\Omega x \ ; \ g(t) = \cos\omega t; \qquad \text{with } \Omega = \frac{\omega}{c}. \tag{3}$$

Gourinat Y, et al., J Radiol Clin Imaging 2024
DOI:10.26502/jrci.2809102

We then apply the following boundary conditions:

$$f(0) = f(L) \ ; \ f'(0) = f'(L), \tag{4}$$

corresponding respectively to continuity in displacement and normal stress. This gives us the following system of equations:

$$\begin{cases} A(1-\cos(\Omega L)) - B\sin(\Omega L) &= 0 \\ A\sin(\Omega L)) + B(1-\cos(\Omega L)) &= 0 \end{cases} \tag{5}$$

Singularity

For the system to have a non-zero solution, its determinant must be zero. The various modes are therefore:

$$\omega_n = 2n\pi\frac{c}{L}, \ n \in \mathbb{N}. \tag{6}$$

This corresponds to a system of standing waves.

We then put together a number of solutions for different discontinuities in closure with the aim of modelling a pathology (see Table 1). The term free refers to the fact that any value of the given magnitude would satisfy the boundary conditions. You will find a representation of each case carried out with Julia on the Fig 2. The amplitudes of the longitudinal displacements are plotted as transverse displacements for better visualisation:

- The first case in the table corresponds to the one we treated earlier. The fact that A and B are free simply implies that the standing wave for a given frequency has all possible phase shifts.
- The second case is that of a Möbius inversion of the normal force. In this case, any frequency gives a valid standing wave solution with a fixed phase. This is very interesting in that it can model absolute noise in the solution.
- The third case is that of a Möbius inversion on the normal force to which we add a constant parameter ν. The only admissible solution is the continuous solution which has an antinode at the closure (zero force).
- The fourth case is that of a parametric inversion ε with the addition of a parameter ν on the normal effort. The only solution is similar to the previous case.
- The fifth case is that of a displacement discontinuity parametrised by δ and an effort discontinuity parametrised by ε. This case is only valid for certain values of the pair δ, ε. This case admits discontinuous solutions for frequencies depending on the pair of parameters.
- The sixth case is that of a simple discontinuity in displacement parametrised by δ. The admissible solution is the continuous solution with a node at the closure (zero displacement).
- The seventh case is that of a Möbius inversion on displacement. The frequency behaviour of the case of Möbius inversion under normal load is repeated.
- The last case is that of a double Möbius inversion in displacement and effort. The solution does present a discontinuity for certain frequencies and its phase is not fixed.

Table 1: Catalogue of solutions for Ring Beams

Conditions		Results of U		
f	$N \to f'$	Ω	A	B
$f(0) = f(L)$	$f'(0) = f'(L)$	$\frac{2\pi n}{L}$	*free*	*free*
$f(0) = f(L)$	$f'(0) = -f'(L)$	*free*	$\begin{cases} 0 \text{ if } \Omega = \frac{(2n+1)\pi}{L} \\ \text{free o/w} \end{cases}$	$\begin{cases} \text{free if } \Omega = \frac{(2n+1)\pi}{L} \\ \left(\frac{\sin}{\cos+1}\right)(\Omega L)\ A \ \text{ o/w} \end{cases}$
$f(0) = f(L)$	$f'(0) = -f'(L) + \nu, \ \nu \in \mathbb{R}^*$	$\frac{2\pi n}{L}$	*free*	$\frac{\nu}{2\Omega}$
$f(0) = f(L)$	$f'(0) = \varepsilon f'(L) + \nu, \ \varepsilon \notin \{-1,1\}, \ \nu \in \mathbb{R}$	$\frac{2\pi n}{L}$	*free*	$\frac{\nu}{(1-\varepsilon)\Omega}$
$f(0) = \delta f(L)$	$f'(0) = \varepsilon f'(L), \ \begin{matrix} -1 < \varepsilon < 1, \ \delta \geq 1 \\ \text{or} \\ \begin{cases} -1 \leq \delta \leq 1, \ \varepsilon > 1 \\ \delta \neq 0 \end{cases} \end{matrix}$	$\frac{1}{L}\cos^{-1}\left(\frac{\delta\varepsilon+1}{\delta+\varepsilon}\right)$	*free*	$\pm\frac{\varepsilon}{\delta}\sqrt{\frac{1-\delta^2}{\varepsilon^2-1}}A$
$f(0) = \delta f(L)$	$f'(0) = f'(L), \ \delta \notin \{-1,1\}$	$\frac{2\pi n}{L}$	0	*free*
$f(0) = -f(L)$	$f'(0) = f'(L)$	*free*	$\begin{cases} \text{free if } \Omega = \frac{(2n+1)\pi}{L} \\ \left(\frac{-\sin}{\cos+1}\right)(\Omega L)\ B \ \text{ o/w} \end{cases}$	$\begin{cases} 0 \text{ if } \Omega = \frac{(2n+1)\pi}{L} \\ \text{free o/w} \end{cases}$
$f(0) = -f(L)$	$f'(0) = -f'(L)$	$\frac{(2n+1)\pi}{L}$	*free*	*free*

Gourinat Y, et al., J Radiol Clin Imaging 2024
DOI:10.26502/jrci.2809102

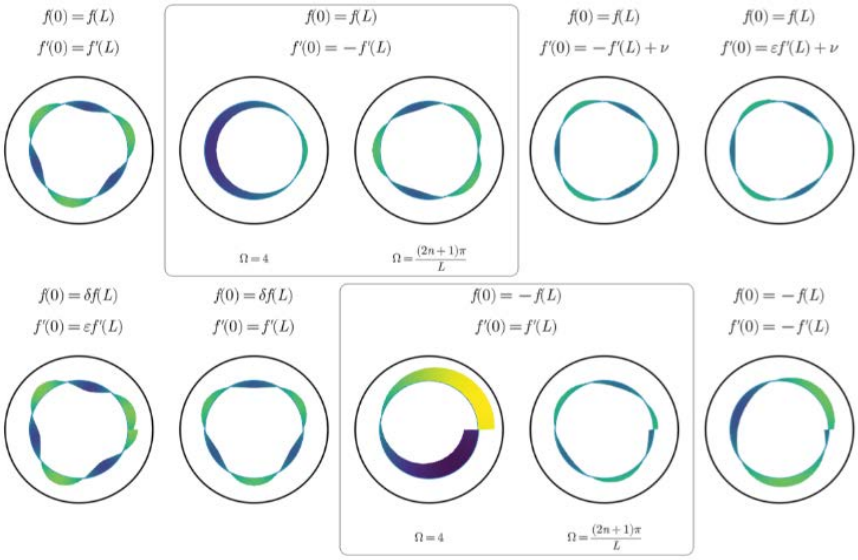

Figure 2: Visualisation of the amplitudes of longitudinal displacement for various cases

This preliminary study reveals the interesting case of a Möbius inversion on a junction that leads to frequency noise. This could be used to model a pathology such as tinnitus.

Canal Segmented Model

Model of a Healthy Ear

The anterior semicircular canal is modelled as a succession of 3 beams that are closed topologically. The first one corresponds to the utricle and ampulla system. The second one corresponds to the anterior SCC and the third one models the common crus between the anterior and posterior SCCs.

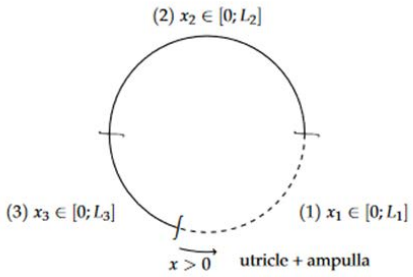

$$\forall (i,j) \in \{1;2;3\}^2,\ \begin{cases} E_i = E_j \\ \rho_i = \rho_j \end{cases} \implies \boxed{\Omega_i = \Omega_j} \tag{7}$$

We also have the following relation between the natural pulses of different parts of the canal:

which will be the case for our model.

The contribution of the posterior SCC is modelled by a normal force discontinuity at beam 3 (common crus):

$$\varepsilon N_1(0) = N_3(L_3)\ ;\ \delta N_3(0) = N_2(L_2). \tag{8}$$

In the same way as in the previous section, we will apply the boundary conditions for the model of the healthy inner ear, and analyse the analytical solutions -- indeed, in this more complicated model, the majority of solutions are purely numerical.

$$\text{Conditions}: \boxed{\begin{array}{ll} f_1(0) = f_3(L_3) & \varepsilon N_1(0) = N_3(L_3) \\ f_2(0) = f_1(L_1) & N_2(0) = N_1(L_1) \\ f_3(0) = f_2(L_2) & \delta N_3(0) = N_2(L_2) \\ E_1 = E_2 = E_3 & \rho_1 = \rho_2 = \rho_3 \end{array}}; \tag{9}$$

$$\text{where } N_i = E_i S_i \frac{\partial U_i}{\partial x} = E_i S_i g_i f_i'.$$

Gourinat Y, et al., J Radiol Clin Imaging 2024
DOI:10.26502/jrci.2809102

Pathological configuration

Pathology can be modelled by a discontinuity within the anterior SCC. A discontinuity in displacement and normal effort is applied

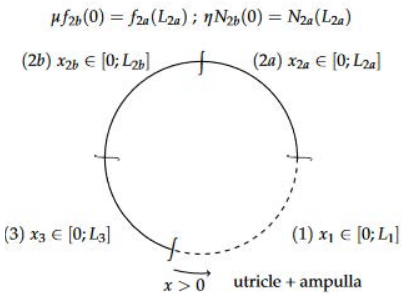

(10)

The dehiscence is generally located between a third and two thirds of the anterior SCC, starting from the ampulla.

We will apply the following boundary conditions:

$$\begin{array}{rr} f_1(0) = f_3(L_3) & \varepsilon N_1(0) = N_3(L_3) \\ f_{2a}(0) = f_1(L_1) & N_{2a}(0) = N_1(L_1) \\ \mu f_{2b}(0) = f_{2a}(L_{2a}) & \eta N_{2b}(0) = N_{2a}(L_{2a}) \\ f_3(0) = f_{2b}(L_{2b}) & \delta N_3(0) = N_{2b}(L_{2b}) \\ E_1 = E_{2a} = E_{2b} = E_3 & \rho_1 = \rho_{2a} = \rho_{2b} = \rho_3 \end{array}$$

Anatomical Data

The data we are using comes from references [1] to [4]. These are approximate values for an anterior SCC. We take the density of water, as we are studying biological tissues. The radius of curvature is approximately R = 4.0 mm while the slender duct cross-sectional radius is approximately r = 0.19 mm. We will therefore assume that R ≫ r.

i	L_i (mm)	S_i (mm^2)	ρ_i (kg/m^3)	E_i (Pa)	c_i (m/s)
1	7.20	1.40	1000	$2 \cdot 10^3$	$\sqrt{\frac{E_1}{\rho_1}} = 1.41$
2 [2a + 2b]	16.86 [5.62 + 11.24]	0.11	1000	$2 \cdot 10^3$	1.41
3	3.54	0.52	1000	$2 \cdot 10^3$	1.41

In the physiological case, the pressure variation amplitude of the SCC are on the order of 1nPa - 1µPa and contribute very little to the dynamics of the inner ear, and can thus be mostly discarded. The SCC also does not contribute to the ear's sound perception, as sound is only perceived in the cochlea.

In the case of the dehiscence, the dynamics of the SCC become much more prevalent, with pressure variations in the order of 10µPa ~ 100µPa REF. In this case, because of the third window, vibrations in the SCC have a much greater impact on the dynamics of the inner ear and notably the cochlea, meaning vibrations caused by sound outside sound will cause vibration in the SCC (which could lead to conditions like vertigo, loss of balance, ...).

In addition, with the opening of the third window, addition vibrations will come from the interior of the body, which will cause vibrations in the SCC, thus affecting the cochlea and creating a phenomenon of autophony. The dynamics of the SCC thus become fundamental in the dynamics of the whole inner ear, as the amplified vibrations could create tinnitus. On the other hand, vibration damping in the dynamics of the SCC could create a loss of hearing in certain frequency bands.

Gourinat Y, et al., J Radiol Clin Imaging 2024
DOI:10.26502/jrci.2809102

Related pathologies are described in the following table:

pathology	Causes	Consequences
Dehiscence (DCS)	The absence of the thin layer of bone covering the superior semicircular canal causes disruption of the hair cells of the semicircular canals by sound waves	Dizziness (sound-induced (Tullio), pressure-induced (Hennebert), tilting sensation) Imbalances Nystagmus
Labyrinthitis	Viral infection due to an opening between the middle ear and the inner ear due to increased pressure as well as Inflammation (edema)	Vertigo (Feeling of spinning or moving while the person is still. Can be severe and disabling, often associated with sudden head movements.) Imbalance and difficulty walking (Coordination and stability problems, Feeling "pitching" or "rocking" when walking) Sensation of ear fullness (Feeling of pressure or congestion in the ear) Nystagmus
Perilymphatic Fistula	Opening between the middle ear and the inner ear which causes perilymph to leak from the semi-circular canals into the middle ear	Vertigo and imbalance (Episodes of vertigo (sensation of rotation or movement often triggered by physical exertion, changes in pressure, or movements of the head), Imbalance and instability Sensitivity to changes in pressure (symptoms exacerbated by activities increasing intracranial pressure, such as coughing, sneezing, or lifting weights) Sensation of ear fullness Nystagmus

Application And Discussion

Model implementation in physiological configuration.

Applying the boundary conditions, we have the following system:

$$\begin{cases} -A_1 & -A_1\cos(\Omega L_1) & -B_1\sin(\Omega L_1) & +A_2 & & & -A_3\cos(\Omega L_3) & -B_3\sin(\Omega L_3) & = 0 \\ & & & -A_2\cos(\Omega L_2) & -B_2\sin(\Omega L_2) & +A_3 & & & = 0 \\ & & B_1S_1\Omega\varepsilon & & & +A_3S_3\Omega\sin(\Omega L_3) & -B_3S_3\Omega\cos(\Omega L_3) & & = 0 \\ & A_1S_1\Omega\sin(\Omega L_1) & -B_1S_1\Omega\cos(\Omega L_1) & & +B_2S_2\Omega & & & & = 0 \\ & & & A_2S_2\Omega\sin(\Omega L_2) & -B_2S_2\Omega\cos(\Omega L_2) & & & +B_3S_3\Omega\delta & = 0 \end{cases} \tag{11}$$

The nullity of the determinant in this system allows us to find simple solutions. Here are a few of them:

	$\Omega_i L_i$			A_i			B_i		
(1)	$n_1\pi$	$n_2\pi$	$n_3\pi$	*free*	$(-1)^{n_1}A_1$	$(-1)^{n_3}A_1$	*free*	$(-1)^{n_1}\frac{S_1}{S_2}B_1$	$(-1)^{n_3}\frac{S_1}{S_3}\varepsilon B_1$
(2)	$\left(n_1+\frac{1}{2}\right)\pi$	$\left(n_2+\frac{1}{2}\right)\pi$	$\left(n_3+\frac{1}{2}\right)\pi$	*free*	$\delta(-1)^{n_2+1}\frac{S_3}{S_2}B_3$	$(-1)^{n_2}B_2$	$(-1)^{n_1}A_2$	$(-1)^{n_1+1}\frac{S_1}{S_2}A_1$	$(-1)^{n_3}A_1$
(3)	$n_1\pi$	$n_2\pi$	$\left(n_3+\frac{1}{2}\right)\pi$	*free*	$(-1)^{n_1}A_1$	$(-1)^{n_2}A_2$	$(-1)^{n_1}\frac{S_2}{S_1}B_2$	$\delta(-1)^{n_2}\frac{S_3}{S_2}B_3$	$(-1)^{n_3}A_1$
(4)	$\left(n_1+\frac{1}{2}\right)\pi$	$n_2\pi$	$\left(n_3+\frac{1}{2}\right)\pi$	*free*	$(-1)^{n_1}B_1$	$(-1)^{n_2}A_2$	*free*	$(-1)^{n_1+1}\frac{S_1}{S_2}A_1$	$(-1)^{n_3}A_1$

We can further find through relation 7,

$$\forall(i,j)\in\{1;2;3\}^2,\ \frac{\Omega_i L_i}{L_i}=\frac{\Omega_j L_j}{L_j}\implies\frac{L_i}{L_j}=\frac{\Omega_i L_i}{\Omega_j L_j}=\frac{n_i+\frac{1\pm1}{4}}{n_j+\frac{1\pm1}{4}},$$

Gourinat Y, et al., J Radiol Clin Imaging 2024
DOI:10.26502/jrci.2809102

which will provide another relation between the ratio of the lengths Li and a ratio of integers with varying parities depending on the case being treated. This will limit the amount of cases which would actually be viable in practice given the set lengths Li, and even more so were we to only consider low frequency cases – the higher frequency pulses being damped by the various low-pass filters created by the body's tissues.

$$
\begin{aligned}
&(1)\quad \text{following} \quad \begin{cases} n_1+n_2+n_3 \equiv 0 \pmod 2 \\ \varepsilon\delta = 1 \\ \forall (i,j) \in \{1;2;3\}^2,\ \dfrac{L_i}{L_j} = \dfrac{n_i}{n_j} \end{cases} \Longrightarrow\ n_1 \approx 4k, n_2 \approx 8k, n_3 \approx 2k, k \in \mathbb{N} \\
&(2)\quad \text{following} \quad \begin{cases} \varepsilon\delta = -1 \\ \forall (i,j) \in \{1;2;3\}^2,\ \dfrac{L_i}{L_j} = \dfrac{2n_i+1}{2n_j+1} \end{cases} \\
&(3)\quad \text{following} \quad \begin{cases} \varepsilon\delta = -1 \\ \dfrac{L_1}{L_2} = \dfrac{n_1}{n_2} \\ \dfrac{L_1}{L_3} = \dfrac{2n_1}{2n_3+1} \end{cases} \Longrightarrow\ n_1 \approx 3, n_2 \approx 6, n_3 \approx 1 \\
&(4)\quad \text{following} \quad \begin{cases} \dfrac{S_1}{S_3} = \delta(-1)^{k_1+k_2+k_3+1} \\ \varepsilon\delta = 1 \\ \dfrac{L_1}{L_2} = \dfrac{2n_1+1}{2n_2} \\ \dfrac{L_2}{L_3} = \dfrac{2n_2}{2n_3+1} \end{cases}
\end{aligned}
$$

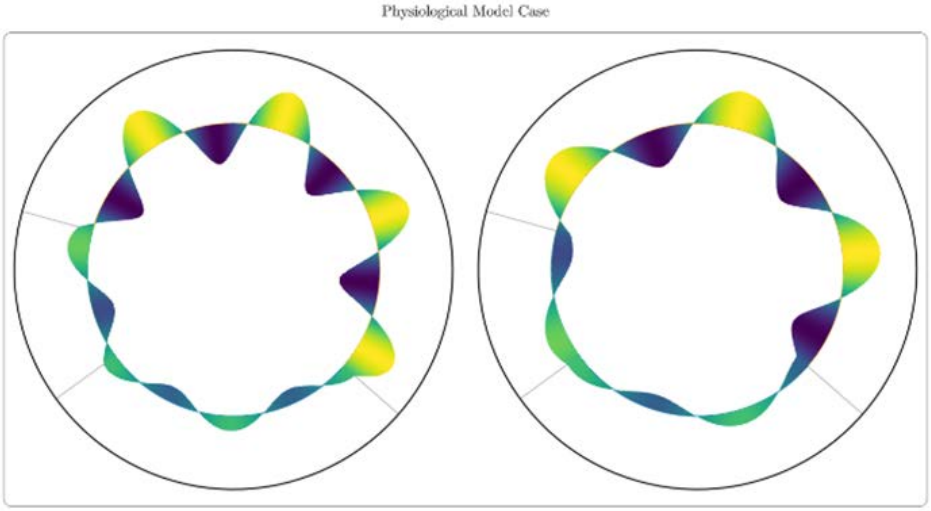

Figure 3: Visualisation of the amplitudes of longitudinal displacement for example Physiological Model cases

Shown above in figure 4 are screen captures of the cases (1) and (3) animated in Julia, for arbitrary A1 and B1. We can notice discontinuities in the slopes of the normal displacement, which are a result of the varying cross sections of the different beams, regardless of the values of δ and ε.

We ought to be careful using these visualisations as the displacement represented here radially is actually a longitudinal displacement. This representation was chosen for the sake of legibility.

Model implementation in pathological configuration

As in the physiological case, there are simple modal solutions which are only possible under certain conditions (see table below).

Gourinat Y, et al., J Radiol Clin Imaging 2024
DOI:10.26502/jrci.2809102

$\Omega_i L_i$				A_i				B_i			
$n_1\pi$	$n_{2a}\pi$	$n_{2b}\pi$	$n_3\pi$	$(-1)^{n_3}A_3$	$(-1)^{n_1}A_1$	$(-1)^{n_{2a}}\frac{1}{\mu}A_{2a}$	free	$(-1)^{n_3}\frac{S_3}{S_1}\frac{1}{\varepsilon}B_3$	$(-1)^{n_1}\frac{S_1}{S_{2a}}B_1$	$(-1)^{n_{2a}}\frac{S_{2a}}{S_{2b}}\frac{1}{\eta}B_{2a}$	free
$n_1\pi$	$n_{2a}\pi$	$n_{2b}\pi$	$\left(n_3+\frac{1}{2}\right)\pi$	$(-1)^{n_3}B_3$	$(-1)^{n_1}A_1$	$(-1)^{n_{2a}}\frac{1}{\mu}A_{2a}$	$(-1)^{n_{2b}}A_{2b}$	$(-1)^{n_3+1}\frac{S_3}{S_1}\frac{1}{\varepsilon}A_3$	$(-1)^{n_1}\frac{S_1}{S_{2a}}B_1$	$(-1)^{n_{2a}}\frac{S_{2a}}{S_{2b}}\frac{1}{\eta}B_{2a}$	free
$n_1\pi$	$n_{2a}\pi$	$\left(n_{2b}+\frac{1}{2}\right)\pi$	$\left(n_3+\frac{1}{2}\right)\pi$	$(-1)^{n_3}B_3$	$(-1)^{n_1}A_1$	$(-1)^{n_{2a}}\frac{1}{\mu}A_{2a}$	free	$(-1)^{n_3+1}\frac{S_3}{S_1}\frac{1}{\varepsilon}A_3$	$(-1)^{n_1}\frac{S_1}{S_{2a}}B_1$	$(-1)^{n_{2a}}\frac{S_{2a}}{S_{2b}}\frac{1}{\eta}B_{2a}$	free
$n_1\pi$	$\left(n_{2a}+\frac{1}{2}\right)\pi$	$\left(n_{2b}+\frac{1}{2}\right)\pi$	$\left(n_3+\frac{1}{2}\right)\pi$	$(-1)^{n_3}B_3$	$(-1)^{n_1}A_1$	$(-1)^{n_{2a}}\frac{1}{\mu}B_{2a}$	$(-1)^{n_{2b}}B_{2b}$	$(-1)^{n_3+1}\frac{S_3}{S_1}\frac{1}{\varepsilon}A_3$	$(-1)^{n_1}\frac{S_1}{S_{2a}}B_1$	$(-1)^{n_1+n_{2a}+n_3+1}\frac{S_{2a}}{S_{2b}}\frac{1}{\eta}B_3$	free

(1) following $(-1)^{n_1+n_{2a}+n_{2b}+n_3}=\mu=\delta\varepsilon\eta$ with $\begin{cases} n_1\approx 4, n_{2a}\approx 4, n_{2b}\approx 4, n_3\approx 2 \text{ if } \mu=1 \\ n_1\approx 2, n_{2a}\approx 2, n_{2b}\approx 2, n_3\approx 1 \text{ if } \mu=-1 \end{cases}$

(2) following $\delta\varepsilon\eta\mu=-1$ with $n_1\approx 3, n_{2a}\approx 3, n_{2b}\approx 3, n_3\approx 1$

(3) following $(-1)^{n_1+n_{2a}+n_{2b}+n_3+1}=\varepsilon\eta\frac{S_{2b}}{S_3}=\delta\mu\frac{S_3}{S_{2b}}$

(4) following $\delta\varepsilon\eta\mu=-1$

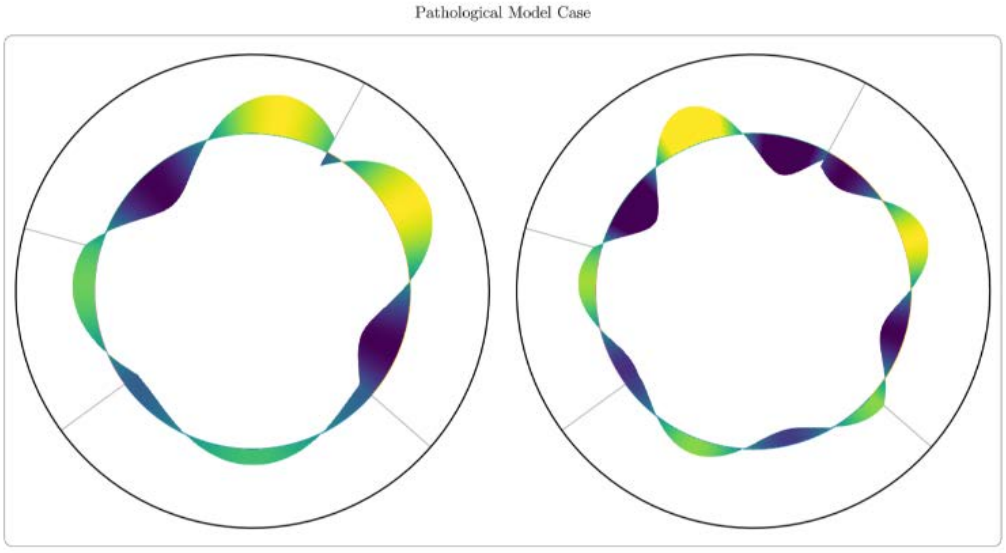

Figure 4: Visualisation of the amplitudes of longitudinal displacement for example Pathological Model cases

Cases (1) and (2) are represented in the visualisation above. As expected, the analytical solutions provide a way to model the discontinuities both in displacement and pressure (through displacement derivative). We can now use these solutions to model different pathologies which correspond themselves to different discontinuities.

To fully understand the effect of these pathologies we can now exploit the frequency spectra of the model.

Frequency Response Function

The following results show the impact of the different conditions, described above, on the SCC's dynamics modelled as a discontinuity on either or both pressure or displacement.

Gourinat Y, et al., J Radiol Clin Imaging 2024
DOI:10.26502/jrci.2809102

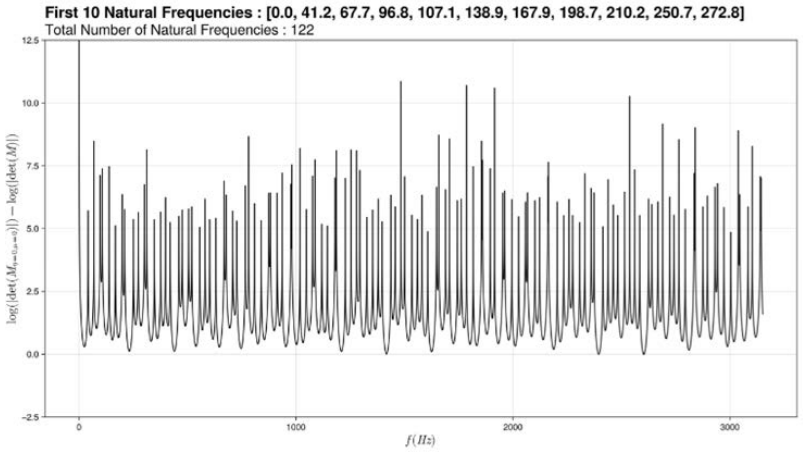

Figure 5: Model Graph of Semi-circular canals for a healthy ear

We traced frequency response function modelling the resonant frequencies of semicircular canals. We then obtain graphs of the log of the determinant of the system as a frequency response function in Hz, as a way to detect the zeros of the determinant corresponding to spikes towards infinity -- the spikes not seeming to shoot to infinity being a simple artifact of the generously discrete nature of the frequency. We have chosen to include in its graphs 2 cursors: one on the discontinuity in viscosity and one on the spatial discontinuity. For a healthy ear, we thus get the graph above. A first deduction would be that semicircular canals react to audible frequencies.

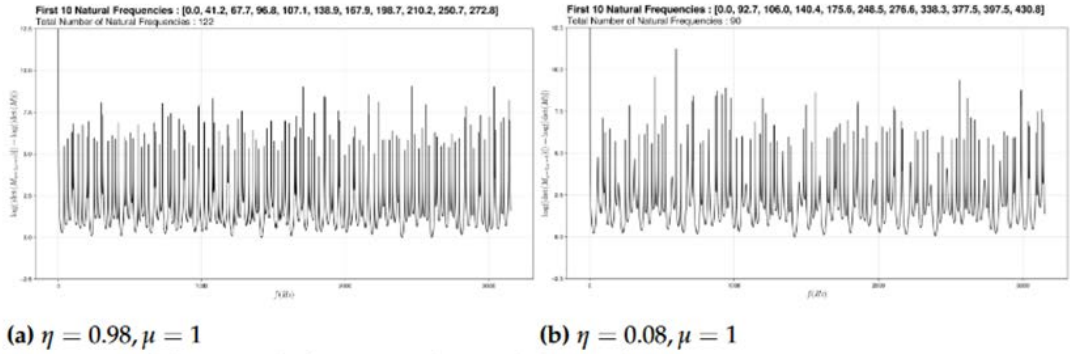

Figure 6: Modeling graph of semi-circular canals for a sick ear

We notice that if we vary only slightly the η (pressure discontinuity) nothing happens at the graph level but if this change is more important, we have a loss of the lower frequencies.

We have linked this graph to dehiscence. Indeed, in the physiological case, the sound waves have no impact on the ciliated cells of the semicircular channels because their amplitudes are insufficient (some μ to mPa) which is modelled here by the small variation of the η. Whereas in the pathological case, the sound waves are amplified (0.01Pa - 0.1Pa) by the hole present above the channels. The variation of the η is therefore more important. The sound waves impact the hair cells of the channels.

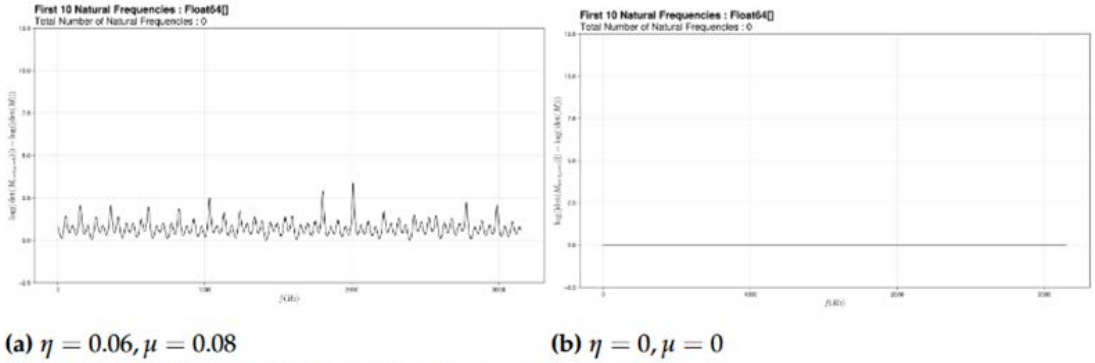

Figure 7: Modeling graph of semi-circular canals for a sick ear

Gourinat Y, et al., J Radiol Clin Imaging 2024
DOI:10.26502/jrci.2809102

For this first sub graph, we varied the η (discontinuity on pressure) and the μ (discontinuity of displacement). This has been associated with labyrinthitis since we have assimilated edema to a more or less important obstruction and have coupled this obstruction to the increase in pressure that causes this pathology. And if this phenomenon increases, this third graph is obtained. In this case, no matter the external vibrations, nothing reacts. The last graph represents the case where there is a loss of pressure within the system.

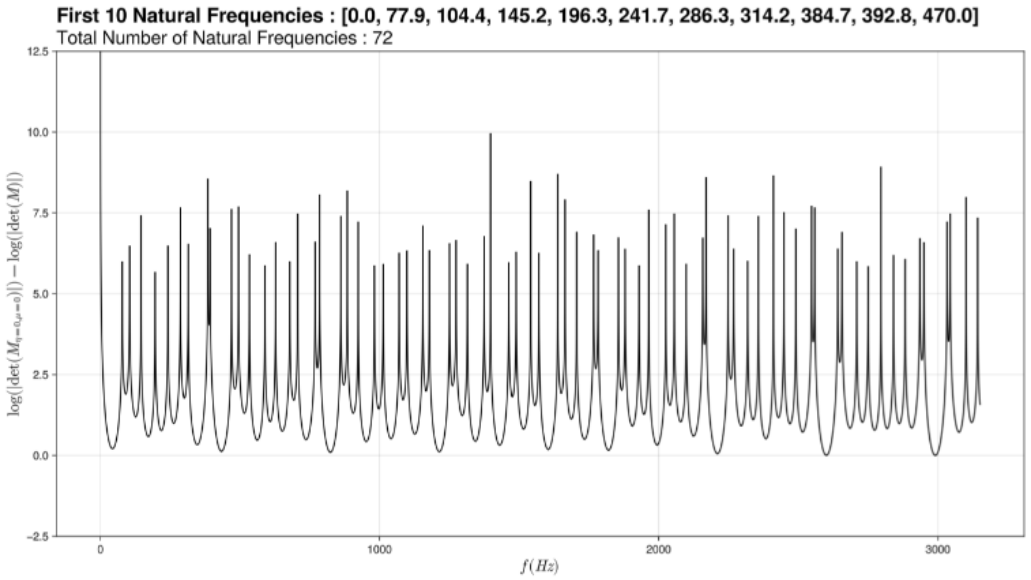

Figure 8: Modeling graph of semi-circular canals for a sick ear

This graph was plotted for a η negative which means there would be a loss of pressure. We have connected this with a perilymphatic fistula since it is due to a loss of fluid from the inner ear to the middle ear and therefore a loss of pressure in the inner ear.

Conclusion and Perspectives

Robustness and predictivity

The 1D physiological model - elementary or segmented - accounts for longitudinal deformable modes in the canal - in fluid/solid environment interaction since the material is median. An essential result of this generic solution is the dimensional convergence of relative segment lengths to integer ratios, in the form of simple fractions that are actually observed anatomically. This is a convincing result of the natural optimization of these canals, which has been observed here particularly in the anterior canal.

The 1D pathological model, in which a passive singularity (Eulerian pressure discontinuity) or an active singularity (local Möbius inversion) generates different disturbances. In one case out of two, more than half of the constants given by the boundary conditions become indeterminate, i.e. we may have a free or random solution. Mathematically, this type of disturbance can induce modal noise in the channel's behaviour. We have here an opening towards vestibular tinnitus and also towards the possible subsequent controllability of these terms by additional boundary conditions.

Finally, the proposed approach allows discrete modelling of local or global disturbances, relatively robust in terms of global dynamics. This concerns both the pathology represented by a singularity (passive or active) and the damping entropy, developed per segment. On these two points, the proposed model represents a robust approach to both representation and prediction.

Future applications and extensions

Vestibular modeling on acoustic frequencies opens up a path towards weak coupling between auditory and balance acquisitions. While vestibular numerical models are well known, as are cochlear models, coupling matrices between the two are little explored. Models of this type may offer a way forward.

This is a relatively unexplored area, and the proposed model is a breakthrough in the field. In particular, we observe that material elements - fluids and solids - have similar characteristics in the cochlea and vestibule, and that vestibular pathologies

Gourinat Y, et al., J Radiol Clin Imaging 2024
DOI:10.26502/jrci.2809102

can interact - positively or negatively - with those of the cochlea, and vice versa. The model discussed here effectively takes into account the acoustic capabilities of the semicircular canal.

In addition, the 1D model can also, by extension, lead to a transverse structural model (1.5 D bending) potentially carrying four types of singularities. This opening towards fourth-order structural equations could enrich the approach and include hybrid pathologies in particular.

In concrete terms, the modelled bar is based on the equation EU^"-ρU¨=0, of order two, whose generic solution - in terms of shape function – is harmonic, namely f(X)=A cosΩX+B sinΩX [(A,B)∈R^2,Ω∈R^(+*)]. Transverse bending displacement is represented by the equation EIV""+ρSV ¨=0, of fourth order, whose generic solution is both circular and hyperbolic: f(X)=A cosΩX+B sinΩX+C chΩX+D shΩX[(A,B,C,D)∈R^4,Ω∈R^(+*)] is type of solution enables representations possibly extended to other structural modes and other types of singularities.

Declarations

Authors' contributions

Conceptualization, Y.G.; methodology, Y.G.; validation, Y.G. and Q.L; formal analysis, A.R., T.H. and M.-S. G.; investigation, A.R., T.H. and M.-S. G.; resources, Q.L.; data curation, A.R.; writing---original draft preparation, A.R., T.H. and M.-S. G.; writing---review and editing, Y.G.; visualization, A.R.; supervision, Y.G.; project administration, Y.G.. All authors have read and agreed to the published version of the manuscript.

Conflicts of interest

The authors declare that they have no known competing financial interests or personal relationships that could have appeared to influence the work reported in this paper.

Acknowledgements

We thank Manon BLAISE for her brilliant PhD about numerical modelling of semi-circular canals.

References

1. Johnson Chacko L. et al., Analysis of Vestibular Labyrinthine Geometry and Variation in the Human Temporal Bone. Front. Neurosci 12 (2018): 107.
2. Lee JY. A Morphometric Study of the Semicircular Canals Using Micro-CT Images in Three-Dimensional Reconstruction Anat. Rec 296 (2013): 834-839.
3. Iversen M, Rabbitt R. Wave Mechanics of the Vestibular Semicircular Canals, Biophys. J 113 (2017): 1133-1149.
4. David R. Supplementary Information for: Assessing morphology and function of the semicircular duct system: introducing new in-situ visualization and software toolbox. Sci. Rep (2016)
5. Piton J, Négrevergne M, Portmann D. Dehiscence of the superior semicircular canal: Approach and CT scan classifications. Rev. Laryngol. Otol. Rhinol (2008).
6. Philippe Herman. Fistules périlymphatiques. (2024)
7. Mickie Hamiter. Purulent labyrinthitis. (2024).
8. Werner Graf, François Klam. The vestibular system: comparative and functional anatomy, evolution and development. (2024)
9. Docteur Catherine Vidal. Dizziness and disorders of balance. (2024)
10. S. KHARRAT. Dehiscence of the Superior Semi-Circular Canal La Rabta hospital. TUNIS. (2010).
11. Arnaud ATTYEMichael ELIEZER. Towards a generalization of late acquisition for the exploration of cochlear-vestibular disorders in MRI?. (2024).
12. M.DELIAT. Post-traumatic perilymphatic fistulas: etiopathogenesis-diagnosis-treatment University of Limoges (1967).
13. Iversen MM, Zhu H, Zhou W, et al., Sound abnormally stimulates the vestibular system in canal dehiscence syndrome by generating pathological fluid-mechanical waves. Sci Rep 8 (2018): 10257

Gourinat Y, et al., J Radiol Clin Imaging 2024
DOI:10.26502/jrci.2809102

14. Goycoolea MV, Muchow D, Schachern P. Experimental studies on round window structure: Function and permeability. The Laryngoscope. juin 98 (1988):1-20

15. Buck A. The Mechanism of Hearing. Edinb Med J 20 (1874): 468.

16. Minor LB, Solomon D, Zinreich JS, et al., Sound- and/or Pressure-Induced Vertigo Due to Bone Dehiscence of the Superior Semicircular Canal. Arch Otolaryngol Neck Surg 124 (1998): 249.

17. Yuen H, Boeddinghaus R, Eikelboom RH, et al., The Relationship Between the Air-Bone Gap and the Size of Superior Semicircular Canal Dehiscence. Otolaryngol Neck Surg 141(2009): 689-694.

18. Chien W, Ravicz ME, Rosowski JJ, et al., Measurements of Human Middle- and Inner-Ear Mechanics With Dehiscence of the Superior Semicircular Canal. Otol Neurotol. févr 28 (2007): 250-257.